2025 IEEE International Conference on Robotics and Automation (ICRA)
May 19-23, 2025. Atlanta, USA

Automating Tension Calibration for Tendon-Driven Continuum Robots: A Low-Cost Approach Towards Consistent Teleoperation

Kyum Lee[1], Chengnan Shentu[1,3], *Student Member, IEEE,* Chloe Pogue[1,2,3], *Student Member, IEEE,* and Jessica Burgner-Kahrs[1,3], *Senior Member, IEEE*

***Abstract*— We present a low-cost method to automate tension calibration for tendon-driven continuum robots (TDCRs), particularly those lacking tension sensing. Our method utilizes Hall effect sensors to localize the robot's tip with respect to the one-dimensional trajectory it follows under individual tendon actuation. We propose two workflows for robots with and without a static model, making the method generalizable to other tendon-driven soft robots. We demonstrate our method's ability to repeatably tension the tendons through associated tendon displacements. The calibration approach's measured repeatability ($\pm 0.03\,\mathrm{mm}$) is also benchmarked against manual calibration on a TDCR prototype, and its accuracy in achieving target tensions is assessed ($(0.06 \pm 0.20)\,\mathrm{N}$). We further investigate how tension calibration impacts open-loop tracking accuracy, confirming the effectiveness of our method to enhance motion consistency in open-loop control and teleoperation.**

I. Introduction

Violins are meticulously tuned before each performance since the precise tension in the strings is crucial to sound quality. Tendon-driven continuum robots (TDCRs), which feature an elastic backbone actuated by tendons, require an equally precise balance in tendon tension to achieve accurate movements. Repeatable and accurate tension calibration is essential for ensuring optimal performance, particularly in critical applications such as minimally invasive surgery [1].

Joint-level calibration procedures have been widely studied and are ubiquitously implemented in rigid-link robotic systems [2], but remain under-explored in the existing TDCR literature. One potential reason is that TDCR systems have typically been designed for teleoperation applications where an expert operator can compensate for calibration errors via visual feedback [3]. Despite this, inconsistent calibration would force the operators to continuously adapt, making tasks more challenging and physically demanding. Beyond teleoperation, calibration inconsistencies can lead to mismatches with TDCR models during control tasks, introducing actuation delays or dead-band effects.

Motivated by the need to enhance the performance of TDCRs, in this paper we focus on solving the following:

This works was supported in part by the Division of Engineering Science, University of Toronto under the Engineering Science Research Opportunities Program (ESROP-UofT).

[1] Continuum Robotics Laboratory, Department of Mathematical & Computational Sciences, University of Toronto, Mississauga, ON L5L 1C6, Canada. {kyum.lee, c.shentu, chloe.pogue}@mail.utoronto.ca; jessica.burgnerkahrs@utoronto.ca.

[2] Microrobotics Lab, Department of Mechanical and Industrial Engineering, University of Toronto, Toronto, ON M5S 1A1, Canada.

[3] Robotics Institute, University of Toronto, Toronto, ON M5S 0C9, Canada.

Problem Statement ("Tension Calibration"): Given a set of desired tendon tensions $\boldsymbol{T}$, use sensor measurements to find a set of tendon positions, referred to as their home positions, such that the resulting tendon tensions are as close as possible to $\boldsymbol{T}$.

In practice, the desired tendon tensions for all tendons actuating the same segment are usually equal, resulting in a straight TDCR configuration as the home position. Although elastic tendon elongation under tension is often neglected in TDCR modeling due to its minimal impact on accuracy [4], it becomes crucial for the tension calibration problem to ensure a unique solution exists. Given that all fiber materials have a finite yield strength, this problem is well-posed, meaning there is an unique home position for all desired tensions $\boldsymbol{T} > \boldsymbol{0}$. However, modeling and calibrating for specific tendon materials fall outside the scope of this work.

TDCR tension calibration poses some unique challenges compared to rigid-link robots and other types of continuum robots [5]. Firstly, their miniaturized size makes integrating tension sensors in the robot unfeasible, and measurements have to be taken at joint level or in the robot's task-space, complicating accurate tension feedback. Secondly, multiple tendons are attached to a single elastic body, creating tendon coupling, which makes independent calibration of each tendon laborious. Lastly, tendons in tension inevitably experience creep which leads to gradual tension loss over time. This prevents the long-term use of a single tendon tension calibration, requiring frequent recalibration to maintain performance. We hypothesize that a desired tension calibration method should be **repeatable, accurate, automated, low-cost, and generalizable** for frequent calibrations on a wide range of TDCR systems.

II. Related Work

In the following, we discuss the current state of the art concerning the tension calibration problem of TDCRs and other tendon-driven or continuum robots. These methods are broadly categorized based on the location of sensing.

A. Joint-space Sensing for Calibration

The most prevalent method of TDCR tension calibration is through joint level force/torque sensing. The most common type of sensors used for tension calibration are load cells, as implemented in [6], [7], [8]. Tension calibration can be performed by loosening all but one tendon to eliminate coupling effects, drive the tendon until the desired tension is reached, and repeat for all tendons. While effective, the addition of

2025 IEEE International Conference on Robotics and Automation (ICRA) | 979-8-3315-4139-2/25/$31.00 ©2025 CRWN | DOI: 10.1109/ICRA55743.2025.11128689

load cells to each tendon's actuator significantly increases the hardware complexity and cost of TDCR systems. These load cells must possess both high precision for accurate tension calibration and a large range to withstand the full range of tensions experienced during TDCR operation. Furthermore, the load cells require careful calibration to ensure uniform sensing across all actuators. Challenges such as hysteresis, creep, and temperature fluctuations can adversely affect the sensing accuracy, limiting the use of these methods to controlled environments like research labs.

Recent works using *proprioceptive* actuators for TDCRs estimate tendon tension from motor currents [9], [10]. Although tension calibration has not yet been achieved with this class of actuators due to noisy estimates, they show promise for tension calibration and control without the added hardware complexity and cost associated with traditional tension sensors.

Nonetheless, all methods that rely on joint-space sensing lack direct feedback on the TDCR itself since the actuators are located remotely to the TDCR. As a result, these methods cannot compensate for tension loss between the TDCR and the tension sensors, which may occur due to friction forces and mechanical tolerances. These factors can vary over time, particularly with changes in the environment or after long-term operation, which leads to calibration errors.

B. Task-space Sensing for Calibration

In contrast with joint-space tension sensing, task-space sensing is concerned with the pose or position measurements, typically of the robot's end-effector. It has been shown to be effective in calibrating the kinematic parameters of rigid-link robots [2], and has been extended to multi-backbone continuum robots [11], parallel continuum robots [12], and pneumatic soft robots [13]. A wide range of sensing principles can be used for task-space sensing, including visual, inductive, magnetic, and electromagnetic, with a subset of them investigated in [14].

For TDCRs and other tendon-driven robots, consistent and accurate tension across tendons has been shown to improve their repeatability [15] while preventing stability issues like buckling [16]. However, there has been limited research on the use of task-space sensing for automated tension calibration. Most existing methods focus on achieving a target shape (e.g., a straight configuration) while maintaining positive tensions, without prioritizing the accuracy of the actual tensions. For instance, in [17], all tendons are manually tensioned before operating the TDCR, while [18] fixes the tendon-driven robotic hand in the desired shape using a jig, and manually tension the tendons. A method to actively compensate for tendon slack by comparing tendon position with sensed TDCR length during operation was proposed in [19], with extra tendon displacements commanded based on a user-defined parameter.

This limited focus on tension accuracy is likely due to tendon tension calibration being classified as a *level 3 (non-kinematic)* calibration task, which is inherently more complex than calibrating joint offsets (*level 1*) or basic kinematic geometry (*level 2*) [20]. In this case, *level 3* calibration requires the accurate modeling of task-space measurements in relation to tendon tensions. While many static TDCR models establish a relationship between tendon tension and task-space configurations [4], they have yet to be applied in the context of tension calibration.

C. Contribution

Our work proposes and validates a novel method to solve the tension calibration problem for TDCR systems, particularly those without tendon tension sensing capabilities. The main contributions of this paper include: 1) Propose a model-based and a model-free workflow to achieve repeatable, accurate, and automated tendon tension calibration; 2) Design, characterize, and evaluate a low-cost, magnetic tension calibration device; 3) Experimentally evaluate the effect of inconsistent tendon tensions for open-loop control, demonstrating the importance of tension calibration for TDCRs.

III. Tension Calibration Workflow

In this section, we first provide a brief overview of the working principle behind our calibration method. Next, we cover the characterization step necessary to establish the distance to field strength relationship, the modular design of the calibration device, and the proposed calibration procedures.

A. Working Principle

We take advantage of the fact that under quasi-static motion, the robot's tip position has a one-to-one relationship with the tension applied to individual tendons. When a single tendon is actuated while the others are loose, the tip of the TDCR follows a one-dimensional path in task-space. Utilizing a well-established static model in literature [21], we can obtain the expected end-effector positions given a desired set of tendon tensions. The static model also requires the TDCR's mechanical properties, tendon geometry, and direction of gravity during calibration, which we assume to be known.

Since the tip trajectory is one-dimensional, a one-dimensional measurement is sufficient to recover the tip position, and by extension the tendon tension. This simplified relationship between measurement and tension allows the use of less complex sensors and enables empirical identification, eliminating the need for a static model if desired.

Among the viable sensing options, we choose magnetic sensors for the following considerations: 1) Hall effect sensors have centimeter-scale sensing volume, which is sufficient for calibrating most TDCR designs; 2) Magnetic field strength is inversely proportional to the distance cubed, making measurements more accurate; 3) Permanent magnets can be easily added to TDCRs' tip during calibration with negligible effects on their motion; 4) Thanks to their wide commercialization, magnets and Hall effect sensors are low-cost and widely-available.

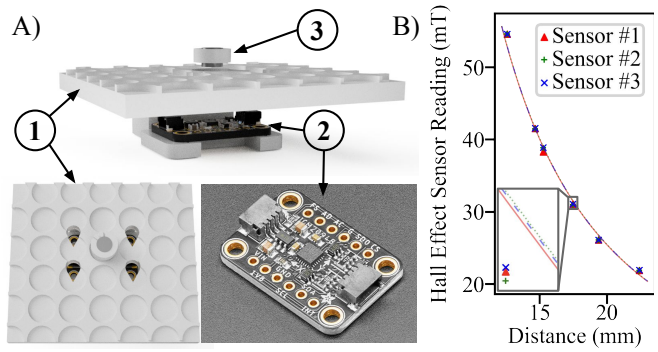

Fig. 1. **Magnetic Characterization Setup:** A) (1) 3D-printed board with circular indentations for the magnet, (2) Adafruit TDK InvenSense ICM-20948 9-DoF IMU with an integrated 3-axis Hall effect sensor, (3) magnet. B) Relationship between the magnetic field reading from the three Hall effect sensors and the distance between the robot's tip magnet and the sensors. The trends for all three Hall effect sensors, shown in red, green, and blue, were highly consistent.

B. Magnet and Hall Effect Sensor Characterization

To determine the distance of the robot's tip-mounted magnet from the Hall effect sensor based on its magnetic readings, we experimentally characterize this relationship with the setup shown in Fig. 1A. The Hall effect sensor (Adafruit TDK InvenSense ICM-20948 9-DoF IMU with an integrated 3-axis Hall effect sensor), which measures magnetic field in the X,Y, and Z directions, was placed at the center of a 3D-printed board with circular indentations. These indentations allowed the magnet to be placed at a known distance from the Hall effect sensor, allowing the field measurement for that distance to be recorded. The measured trend relating Hall effect sensor readings to the distance between the tip magnet and Hall effect sensor is presented in Fig. 1B, which allows for smooth interpolation. This step is repeated for all Hall effect sensors used, and we found the obtained relationships to be consistent. When fitting a power function, the regression factors had around 0.1% variation:

$$\text{Field Strength} = \left\{ \begin{array}{c} 2920.5 \\ 2923.9 \\ 2927.2 \end{array} \right\} \cdot \text{Distance}^{-1.583},$$

This allows us to use the same curve (calculated by the average of the three factors) for all Hall effect sensors. The measured trends deviate from the expected relationship which states that magnetic field strength is inversely proportional to the distance cubed. This could be due to the permanent magnet not being an ideal dipole with zero size, and the close proximity between the magnet and sensors. Influence from nearby ferromagnetic materials and sensor limitations could also skew the relationship.

C. Calibration Device Design

As the proposed calibration method utilizes modular Hall effect sensors, calibration devices can be easily customized for different TDCR systems. We show an example of such a design in Fig. 2A. The device consists of 1) a cylindrical permanent magnet mounted at the center of the tip of the TDCR; 2) a circular array of three Hall effect sensors at the top of the frame, three in this case since there are three tendons per segment; and 3) a 3D-printed frame to accommodate the length of the TDCR and provide the relative position between the TDCR and the Hall effect sensors.

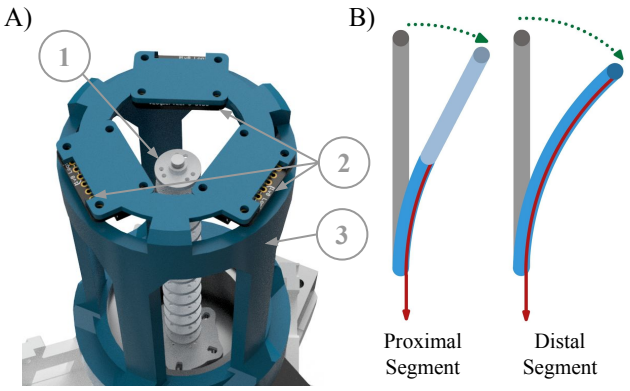

Fig. 2. **Calibration Device:** A) An example calibration device made with low-cost Hall effect sensors and 3D-printed parts. (1) TDCR with tip magnet, (2) Hall effect sensors, (3) 3D-printed frame. B) By measuring tip movement, the device can calibrate TDCRs with different number of segments and tendons.

While the design of the 3D-printed frame is specific to the robot used in this work, its dimensions can be changed to accommodate robots of different lengths and shapes. For every tendon, the Hall effect sensor closest to its target position is selected and used to continuously measure the magnet's relative distance. Their centimeter-scale sensing volume ensures movements in all directions are covered with a minimal number of sensors. Having multiple sensors also allows the compensation of nearby ferromagnetic effects and the earth's magnetic field before each calibration. Key to the simplicity of the design is the ability to calibrate all tendons from one set of Hall effect sensors – Since tendons terminating at any position along the robot will introduce significant tip movement under tension, as illustrated in Fig. 2B, our approach can be used on TDCRs with a different number of segments or different segment designs.

D. Calibration Procedure

We propose both a model-based and model-free tendon tension calibration process, summarized in Fig. 3. Both approaches use the developed calibration device featuring a TDCR with a magnet at its tip, and three Hall effect sensors with known locations (Fig. 2).

For the model-based approach, a static model of the continuum robot is used [21]. The desired tendon tension is given to the model to calculate the expected tip position. Knowing the locations of the Hall effect sensors with respect to the robot, we can determine how close the robot's tip must get to the Hall effect sensors when achieving the desired tendon tension. The magnetic field measurement which corresponds to this distance between the robot's tip magnet and the Hall effect sensor is then set as a target measurement. Next, the

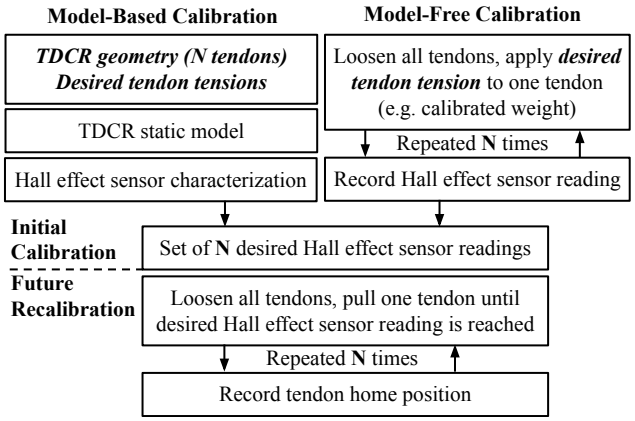

Fig. 3. **Calibration Procedures (*inputs italicized*):** We propose two workflows, model-based and model-free, to obtain a set of desired Hall effect sensor readings. It can then be used for automated and consistent (re)calibration.

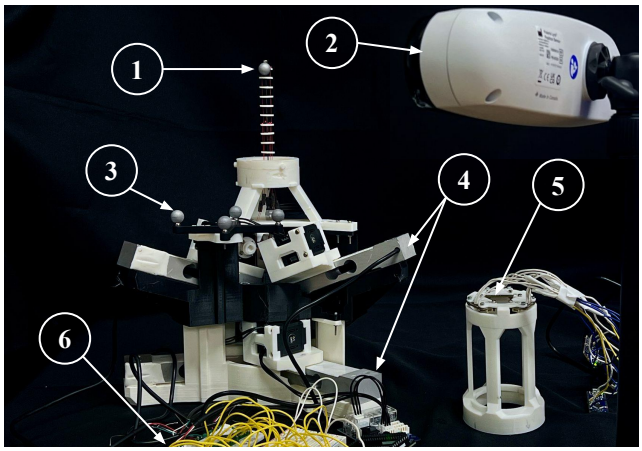

Fig. 4. **Experimental Setup:** (1) TDCR prototype with NDI Polaris Lyra optical marker and magnet at tip, (2) NDI Polaris Lyra optical tracking camera, (3) NDI Polaris Lyra 4-marker rigid body tool, (4) Load cells for tension measurement, (5) Calibration device, (6) HX711 load cell amplifier.

robot's tendon is tensioned using a motor, bending the robot's tip magnet closer to the Hall effect sensor until the target magnetic measurement is reached. The motor's position is recorded and saved as the tendon's home position. This is repeated for all tendons in each of the robot's segments.

The model-free calibration approach bypasses the need for a static continuum robot model and for the magnetic measurement vs. distance characterization. Instead, known weights can be hung from each of the robot's tendons and the corresponding Hall effect sensor measurement can be recorded. This process is repeated for all of the robot's tendons to obtain all desired Hall effect sensor readings. Like in the model-based approach, the motors are used to tension the tendons until the desired Hall effect sensor reading is reached.

As long as the TDCR's dimensions and stiffness remain consistent, the same set of desired tendon tensions will produce the same Hall effect sensor readings. This ensures that the calibration process can be easily repeated, even if components such as tendons or actuators are replaced. Therefore, the proposed calibration workflow is generalizable to a wide range of TDCRs and remains robust despite hardware modifications.

IV. Experimental Results and Discussion

We evaluate the proposed calibration procedure on a two-segment TDCR prototype, in terms of its actuator position repeatability and tension accuracy. We then evaluate the effect of different calibrated tensions for open-loop control.

A. TDCR Prototype

To evaluate our proposed tensioning process, we constructed a two-segment TDCR prototype. The TDCR had a diameter of $12\,\mathrm{mm}$, a segment length of $53\,\mathrm{mm}$, and three tendons per segment (Power Pro Specta Fiber fishing line, $30\,\mathrm{lb}$). Each tendon was actuated by a servo motor (DYNAMIXEL XL430-W250-T) mounted on a load cell (114990100, $0-50\,\mathrm{Kg}$, Seeed Technology Co, Ltd.). The load cells have a ±0.03 percent accuracy, corresponding to approximately $0.15\,\mathrm{N}$ or $15\,\mathrm{g}$. Each load cell was slightly tilted to ensure that the force bearing face of the load cell was perpendicular to the direction of applied tendon tension. This allowed for the direct measurement of the tendon tension as ground truth, which was amplified using six amplifiers (HX711 load cell amplifiers) and digitized by a microcontroller (Arduino Mega).

A small magnet (3.5mm diameter) was mounted on the robot's tip to enable the automatic tensioning process. Three Hall effect sensors (Adafruit TDK InvenSense ICM-20948 9-DoF IMU with an integrated 3-axis Hall effect sensor) were fixed to the 3D-printed calibration device frame, which was then mounted onto the TDCR's base.

An optical tracking system (Polaris Lyra, NDI, RMS $0.2\,\mathrm{mm}$) was also used to obtain ground-truth information for the robot's tip position. An optical marker was fixed to the robot's tip, and the tracking base frame was mounted near the actuators (Fig. 4).

The use of inexpensive components in the calibration device such as three Hall effect sensors ($22 each), three Arduino Nano microcontroller boards for reading measurements ($10 each), a permanent magnet (<$1) and 3D-printed components all made from much less than a single spool of PLA filament ($30) makes this tensioning approach affordable. The total cost of the calibration device is approximately $127 CAD. The cost of the optical tracking system, the load cells, amplifiers, and motors are not included in the total cost of the system as they are not considered to be part of the calibration system.

B. Calibration Repeatability

The calibration repeatability of our automated tensioning approach was compared to that of a manual tensioning approach frequently used in TDCRs. The calibration repeatability evaluates the "closeness" of each motor's absolute position over multiple calibration trials. For this evaluation,

first, each motor's initial position was randomly chosen, resulting in an arbitrary state of "looseness". Next, our automated model-based calibration approach was run with a fixed target tension of $0.8\,\mathrm{N}$. The resulting absolute motor positions for each of the six actuators was recorded.

A similar process was used for manual calibration. First, each motor was powered off and the tendons in the first robot segment were tensioned one at a time. The actuator connected to that tendon was manually turned with a screwdriver until the TDCR deformed slightly in the tendon's direction. This process was repeated for all other tendons in that segment, until the TDCR segment was straight. The "straightness" of the TDCR's body was estimated by visually inspecting the robot's tip position with respect to the calibration device attached, which has a small triangular cutout at its top to provide visual reference. Finally, this process was repeated for the remaining segments until the entire TDCR was straight. The motors were then powered on and their absolute positions recorded.

For both calibration processes, the motor positions (angular) were converted into tendon displacement by multiplying the angle by the tendon spool's radius. The calibration repeatability test was performed 10 times for the automated calibration approach and 5 times for the manual calibration approach. Since the calibrations are performed on the same system consecutively over a short time, we assume no tendon creep and expect the home positions to be constant. The servo motors used have an encoder resolution of 4096 ticks per revolution, which equals to $0.0061\,\mathrm{mm}$. The standard deviation for each of the tendons' displacements were calculated and are presented in Table I.

TABLE I
REPEATABILITY OF TENDON HOME POSITIONS UNDER MANUAL AND AUTOMATED CALIBRATIONS

		Standard Deviation of Home Positions	
Segment #	Tendon #	Manual (mm)	Automated (mm)
1	1	1.941	0.0248
	2	2.503	0.0189
	3	0.991	0.0099
2	1	3.121	0.0089
	2	2.856	0.0066
	3	2.424	0.0726
	Average S.D.	2.408	**0.0328**

The standard deviations from the automated calibration results ($\pm 0.03\,\mathrm{mm}$) are significantly lower than those obtained from the manual calibration ($\pm 2.4\,\mathrm{mm}$). The amount of tension manually applied to each tendon is purely based on the qualitative assessment of the resulting robot deformation against a visual reference. This process is inconsistent as this deflection may differ between tendons and is not quantitatively measured, leading to low repeatability overall. As the manual calibrations were done by the same expert user within a few hours, we expect the repeatability to be worse in practice as calibrations are done over a longer period of time or by different users with different levels of experience.

Furthermore, the automated calibration approach is much faster than the manual approach. Automated calibration took approximately $52\,\mathrm{s}$ per trial whereas manual calibration took between $10\,\mathrm{and}\ 15\,\mathrm{min}$. This highlights the feasibility of automated calibration over the manual method when frequent calibrations are needed (e.g. before each operation).

C. Tension Accuracy

To verify that the automated calibration system can reliably bring each tendon to the desired tension, tests were performed for three different target tensions: 0.5 ,$0.8\,\mathrm{and}\ 1.0\,\mathrm{N}$. The tensioning process was run 5 times for each target tension, and the resulting joint level tension was measured through the installed load cells. The average tendon tensions achieved for all trials is provided in Fig. 5. The average tension error across all tests is $(0.06 \pm 0.20)\,\mathrm{N}$, and tensions are consistent across the two TDCR segments.

Possible sources of error include disturbances affecting the TDCR and sensors, as well as unmodeled effects. Since the target Hall effect sensor readings are obtained from the static model, modeling errors will propagate to the calibration process and contribute to tension errors. Manufacturing tolerances of the TDCR and the calibration device could also introduce errors.

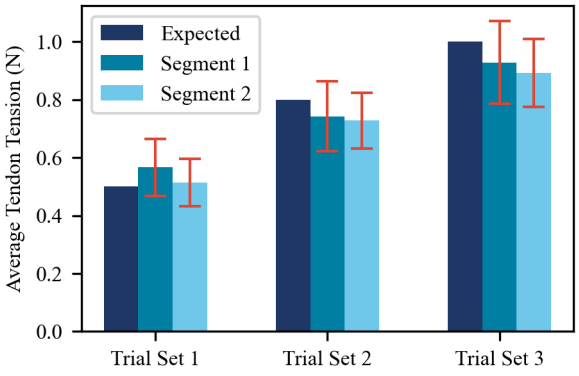

Fig. 5. **Tension Accuracy Evaluation:** The proposed method accurately achieved various target tensions, demonstrating consistent performance across both the proximal and distal TDCR segment.

The limited accuracy of the load cells used in these experiments is a limiting factor for the precision of our tensioning evaluation. The tension measured by the load cells may not exactly reflect the actual tension in the tendons. However, this is a common problem in continuum robot tensioning systems, as load cells have an inherent tradeoff between accuracy and range. This becomes problematic when the load cells are directly used for precise tension calibration for TDCRs that expect high tensions. By using our proposed tensioning approach, we eliminate the need for such load cells, making more accurate tensioning possible without added expenses.

D. Open-loop Tracking Accuracy

To evaluate the effect of tension calibration on TDCRs' motion capabilities, we conducted open-loop control experi-

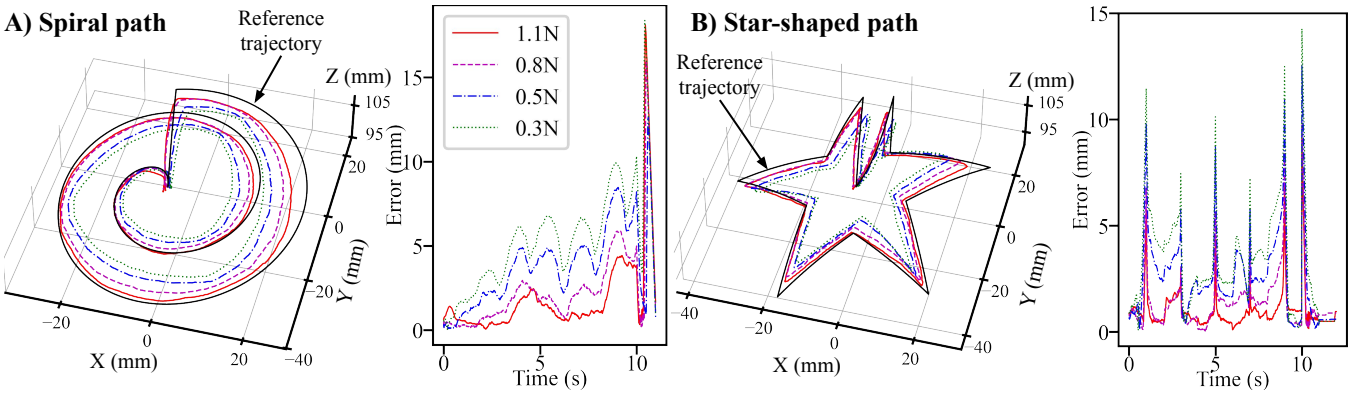

Fig. 6. **Open-loop Evaluation:** The prototype showed significant inconsistency when running identical open-loop commands under different initial tensions. This highlights the importance of frequent and repeatable tension calibration for open-loop tasks as well as developing model-based methods.

ments tracing various trajectories with differing amounts of initial tendon tension: 0.3, 0.5, 0.8, and $1.1\,\mathrm{N}$. This tension was set by the proposed automated calibration process and verified through the installed load cells.

Specifically, two trajectories were tested: a smooth spiral trajectory and a piece-wise linear star-shaped trajectory. The generated tendon actuator commands were sent to all tendons at $100\,\mathrm{Hz}$, and were identical for all four repeated tests per trajectory. The 3D position of the TDCR's tip was measured using the optical tracking system. The trajectory visualizations and tracking errors are presented in Fig. 6. The reference trajectory in task-space, plotted in black, is calculated using constant curvature (CC) forward kinematics as they are commonly used for TDCR teleoperation [22]. As CC is a simplified model, we don't expect the reference trajectory to be followed exactly due to unmodelled effects like gravity and tendon coupling.

For all test runs, there are spikes in tracking error when there is a sharp turn in the trajectories. The trajectories under higher tension showed more precise bending and were overall closer to the reference CC path. Additionaly, we observe that higher tendon tensions achieve more consistent motion across its workspace. The spiral trajectories under $0.3\,\mathrm{N}$ and $0.5\,\mathrm{N}$ showed periodic peaks in error as the TDCR bends in different orientations. This appeared to be caused by insufficient tensions causing the TDCR's motion to be biased towards the physical locations of the tendons.

This significant disparity across trajectories illustrates how a TDCR's open-loop behavior could change drastically under different tensions, even when all tendons are equally tensioned. While more accurate models can be implemented and calibrated to improve open-loop accuracy, a small change in tendon tension could significantly degrade the accuracy of the model. Thus, it is necessary to perform frequent and repeatable tension calibration to ensure the TDCR's consistency for open-loop tasks as well as developing model-based methods.

V. Conclusion and Future Work

In this work, we presented a low-cost, automated method for tension calibration in TDCRs, particularly targeting systems without built-in tension sensing. By using Hall effect sensors to track the robot's tip along a one-dimensional trajectory during individual tendon actuation, we proposed two workflows suitable for both model-based and model-free scenarios. Our method has demonstrated high repeatability (standard deviation of $0.03\,\mathrm{mm}$ in tendon home positions) compared to manual calibration and proven effective in achieving target tensions ($(0.06 \pm 0.20)\,\mathrm{N}$). Additionally, we have shown that proper tension calibration enhances the open-loop accuracy of TDCRs, thereby improving their control and teleoperation capabilities. We will open source the hardware (CAD files, list of electronic components and instructions) as well as code used through the Open Continuum Robotics Project.

For future work, we aim to extend our method to achieve automated parameter calibration (e.g. Young's modulus and Poisson's ratio of the backbone) for TDCRs' static models, which could improve their accuracy in model-based control. Additionally, the identification of tendon properties can be explored to further improve model accuracy and monitor system performance. Although we picked Hall effect sensors as they achieve a good balance between sensing capabilities and cost, our method can be adapted to other sensing modalities. This would further reduce the complexity of TDCR systems if there are existing built-in sensing methods. For instance, some TDCRs have integrated Fiber Bragg Grating sensors or use cameras to measure their shape and tip position. As such, our approach could be adapted to leverage these sensors commonly used in continuum robotics.

References

[1] J. Burgner-Kahrs, D. C. Rucker, and H. Choset, "Continuum robots for medical applications: A survey," *IEEE Transactions on Robotics*, vol. 31, no. 6, pp. 1261–1280, 2015.

[2] J. M. Hollerbach and C. W. Wampler, "The calibration index and taxonomy for robot kinematic calibration methods," *The international journal of robotics research*, vol. 15, no. 6, pp. 573–591, 1996.

[3] P. E. Dupont, N. Simaan, H. Choset, and C. Rucker, "Continuum robots for medical interventions," *Proceedings of the IEEE*, vol. 110, no. 7, pp. 847–870, 2022.

[4] P. Rao, Q. Peyron, S. Lilge, and J. Burgner-Kahrs, "How to model tendon-driven continuum robots and benchmark modelling performance," *Frontiers in Robotics and AI*, vol. 7, p. 630245, 2021.

[5] Q. Boyer, S. Voros, P. Roux, F. Marionnet, K. Rabenorosoa, and M. T. Chikhaoui, "On high performance control of concentric tube continuum robots through parsimonious calibration," *IEEE Robotics and Automation Letters*, 2024.

[6] L. Raimondi, M. Russo, X. Dong, and D. Axinte, "Understanding friction and superelasticity in tendon-driven continuum robots," *Mechatronics*, vol. 104, p. 103241, 2024.

[7] K. Oliver-Butler, J. Till, and C. Rucker, "Continuum robot stiffness under external loads and prescribed tendon displacements," *IEEE Transactions on Robotics*, vol. 35, no. 2, pp. 403–419, 2019.

[8] M. C. Yip and D. B. Camarillo, "Model-less hybrid position/force control: a minimalist approach for continuum manipulators in unknown, constrained environments," *IEEE Robotics and Automation Letters*, vol. 1, no. 2, pp. 844–851, 2016.

[9] Z. Wang and N. M. Freris, "Bioinspired soft spiral robots for versatile grasping and manipulation," *arXiv preprint arXiv:2303.09861*, 2023.

[10] R. M. Grassmann, C. Shentu, T. Hamoda, P. T. Dewi, and J. Burgner-Kahrs, "Open continuum robotics–one actuation module to create them all," *Frontiers in Robotics and AI*, vol. 11, 2024.

[11] L. Wang and N. Simaan, "Geometric calibration of continuum robots: Joint space and equilibrium shape deviations," *IEEE Transactions on Robotics*, vol. 35, no. 2, pp. 387–402, 2019.

[12] K. Nuelle, T. Sterneck, S. Lilge, D. Xiong, J. Burgner-Kahrs, and T. Ortmaier, "Modeling, calibration, and evaluation of a tendon-actuated planar parallel continuum robot," *IEEE Robotics and Automation Letters*, vol. 5, no. 4, pp. 5811–5818, 2020.

[13] C. Escande, T. Chettibi, R. Merzouki, V. Coelen, and P. M. Pathak, "Kinematic calibration of a multisection bionic manipulator," *IEEE/ASME transactions on mechatronics*, vol. 20, no. 2, pp. 663–674, 2014.

[14] V. Modes and J. Burgner-Kahrs, "Calibration of concentric tube continuum robots: Automatic alignment of precurved elastic tubes," *IEEE Robotics and Automation Letters*, vol. 5, no. 1, pp. 103–110, 2019.

[15] Y. Wang, M. McCandless, A. Donder, G. Pittiglio, B. Moradkhani, Y. Chitalia, and P. E. Dupont, "Using neural networks to model hysteretic kinematics in tendon-actuated continuum robots," *arXiv preprint arXiv:2404.07168*, 2024.

[16] Q. Peyron and J. Burgner-Kahrs, "Stability analysis of tendon driven continuum robots and application to active softening," *IEEE Transactions on Robotics*, 2023.

[17] M. Li, R. Kang, S. Geng, and E. Guglielmino, "Design and control of a tendon-driven continuum robot," *Transactions of the Institute of Measurement and Control*, vol. 40, no. 11, pp. 3263–3272, 2018.

[18] Y. Toshimitsu, B. Forrai, B. G. Cangan, U. Steger, M. Knecht, S. Weirich, and R. K. Katzschmann, "Getting the ball rolling: Learning a dexterous policy for a biomimetic tendon-driven hand with rolling contact joints," in *2023 IEEE-RAS 22nd International Conference on Humanoid Robots (Humanoids)*, pp. 1–7, IEEE, 2023.

[19] Y. Fang, X. Dong, A. Mohammad, and D. Axinte, "Design and control of a multiple-section continuum robot with a hybrid sensing system," *IEEE/ASME Transactions on Mechatronics*, vol. 28, no. 3, pp. 1522–1533, 2023.

[20] S. Y. Nof, *Handbook of industrial robotics*. John Wiley & Sons, 1999.

[21] D. C. Rucker and R. J. Webster III, "Statics and dynamics of continuum robots with general tendon routing and external loading," *IEEE Transactions on Robotics*, vol. 27, no. 6, pp. 1033–1044, 2011.

[22] R. J. Webster III and B. A. Jones, "Design and kinematic modeling of constant curvature continuum robots: A review," *The International Journal of Robotics Research*, vol. 29, no. 13, pp. 1661–1683, 2010.